Highlights

A Non-Intrusive Probabilistic Multi-Energy Flow Calculation Method and Its Application in Operation Risk Analysis of Integrated Energy Systems

Bo Dong, Peng Li, Hao Yu, Haoran Ji, Juan Li, Jianzhong Wu, Chengshan Wang

- An sPCE-based non-intrusive probabilistic multi-energy flow model is established.
- A solving algorithm based on Bayesian compressive sensing method is proposed.
- Three violation risk indices based on probabilistic multi-energy flow are constructed.
- A CVaR-based risk analysis method is developed for integrated energy systems.
- The proposed method reduces the computation time by 96% with an acceptable accuracy.

A Non-Intrusive Probabilistic Multi-Energy Flow Calculation Method and Its Application in Operation Risk Analysis of Integrated Energy Systems

Bo Dong[a], Peng Li[a], Hao Yu[a,*], Haoran Ji[a], Juan Li[b], Jianzhong Wu[c] and Chengshan Wang[a]

[a]Key Laboratory of Smart Grid of Ministry of Education, Tianjin University, Tianjin 300072, China
[b]Economic and Technological Research Institute, State Grid Tianjin Electric Power Company, Tianjin 300317, China
[c]Institute of Energy, School of Engineering, Cardiff University, Cardiff CF24 3AA, UK

ARTICLE INFO

Keywords:
Integrated Energy System
Probabilistic Multi-energy Flow Calculation
Sparse Polynomial Chaos Expansion
Operation Risk Analysis
Correlated Uncertainties

ABSTRACT

With the deep coupling of electricity, heat, and gas systems, the uncertainties in renewable energy sources and loads significantly impact the energy flow distribution of integrated energy systems. Probabilistic multi-energy flow calculations considering these uncertain factors have become essential for risk analysis, optimal management, and operational control. However, it is still difficult to efficiently and accurately deal with the diverse and large numbers of correlated random variables. This paper proposes a non-intrusive probabilistic multi-energy flow calculation method and explores its application in the operation risk analysis of integrated energy systems. The probabilistic multi-energy flow model is established considering the uncertainties and correlations of renewable energy sources and loads. The proposed model is solved within the sparse polynomial chaos expansion framework based on Bayesian compressive sensing. Thus, the probabilistic density functions of the risk indices of each subsystem can be obtained. On this basis, the conditional value-at-risk method is employed for the operation risk analysis. The feasibility and advantages of the proposed method are verified using a typical integrated energy system test case.

1. Introduction

An integrated energy system (IES) integrates the production, distribution, conversion, storage, and utilization of multiple energy carriers to realize their coordinated construction and operation [1]. However, the diverse loads and increasing penetration of distributed energy resources have resulted in profound uncertainties in IES [2] . Various uncertainties and fluctuations are propagated and coupled via energy-conversion devices, posing one of the toughest challenges for the operation of an IES. For example, distributed generators with a high correlation may lead to voltage violations in an electric network [3] and disrupt the operation of motors and pumps in other energy networks. The output regulation of a gas power plant may result in fluctuations in its gas consumption and consequently severe pressure disturbances to the gas network [4]. The operational risk of the IES is significantly increased because of the multi-energy interactions and coupled uncertainties. New methods and tools are required to analyze the operation states and risks of an IES under complex operating modes and scenarios.

Multi-energy flow calculations [5, 6] are essential for IES risk analysis as well as many other applications, such as planning [7], optimal dispatch [8, 9], security analysis [10, 11], and dynamic simulation [12]. Nevertheless, conventional multi-energy flow calculation mainly uses deterministic methods, that is, deterministic multi-energy flow (DMEF) calculations. DMEF lacks the ability to deal with uncertainties and cannot efficiently reveal the operation risks caused by fluctuating energy sources and loads, making it difficult to be fully trusted by planners and operators. This problem motivates the adoption of probabilistic multi-energy flow calculation (PMEF) methods, in which uncertainties are handled using a large amount of historical data, statistical results, or analytical modeling approaches [13, 14].

The most representative probabilistic multi-energy flow calculation method is the Monte-Carlo simulation (MCS), which generates numerous random samples and conducts a DMEF calculation for each sample to derive the overall probability distribution of energy flows [15, 16]. However, the accuracy of MCS method is highly dependent on the

⋆This study was supported by the National Natural Science Foundation of China (51907139, 52011530127) and National Postdoctoral Program for Innovative Talents (BX201900229).
*Corresponding author, email: tjuyh@tju.edu.cn
ORCID(s):

Nomenclature

Abbreviations

BCS	Bayesian compressive sensing
CDF	Cumulative distribution function
CVaR	Conditioned Value-at-Risk
DMEF	Deterministic multi-energy flow
gPC	Generalized polynomial chaos
IES	Integrated energy system
LAR	Least angle regression
MCS	Monte Carlo simulation
PDF	Probabilistic density function
PMEF	Probabilistic multi-energy flow
sPCE	Sparse polynomial chaos expansion

Indices

i, j	Indices of nodes
k	Indices of pipelines

Variables

a_i	Expansion coefficients
f	Flow rate of pipeline in gas network
$f_{\delta \mathrm{E}}$	Voltage risk index of electric subsystem
$f_{\delta \mathrm{H}}$	Flow rate risk index of heat subsystem
$f_{\delta \mathrm{G}}$	Pressure risk index of gas subsystem
$F_{b,i}^{\mathrm{in}} / F_{b,i}^{\mathrm{out}}$	ith energy flow enters/leaves bus b
$F_{e,i}^{\mathrm{in}} / F_{e,i}^{\mathrm{out}}$	ith input/output power of equipment e
H	Output power of compressor
$\boldsymbol{J}$	Jacobian matrix
m	Flow rate of pipeline
m_q	Injection flow rate
p_i	Pressure of node i
P_i	Injected active power of node i
Q_i	Injected reactive power of node i
T_s	Supply temperature
T_o	Output temperature
T_r	Return temperature
T_{end}	Temperature of the end node of pipeline
T_{start}	Temperature of the start node of pipeline
U_i	Voltage magnitude of node i
W	Injection heat power
$\boldsymbol{x}$	Random variables
θ_i	Phase angle of node i
$w(\boldsymbol{x})$	Weight function
$\Phi_i(\boldsymbol{x})$	Orthogonal polynomial basis
$\delta_{\mathrm{E}}(i)$	Voltage violation value of node i
$\delta_{\mathrm{H}}(i)$	flow rate violation value of pipeline i
$\delta_{\mathrm{G}}(i)$	Pressure violation value of node i

Parameters

$\boldsymbol{A}_{\mathrm{h}}$	Node-branch matrix of heat system
$\boldsymbol{B}_{\mathrm{h}}$	Loop-branch matrix of heat system
C_{p}	Specific heat capacity
D	Diameter of pipeline
K	Weymouth coefficients
L	Length of pipeline
$m_{i,\max}$	Upper limit of flow rate of pipeline i
n_{E}	Number of electric nodes
n_{H}	Number of heat pipelines
n_{G}	Number of gas nodes
$p_{i,\max} / p_{i,\min}$	Upper/lower pressure limits of node i
P_{n}	Standard atmospheric pressure
r	Expansion order of sPCE
R	Heat transfer coefficient
S	Gas compression ratio
T_n	Standard temperature
T_{a}	Ambient temperature
$V_{i,\max} / V_{i,\min}$	Upper/lower limits of voltage of node i
η_a, η_b, η_c	Energy consumption coefficient
ν, κ, ω, μ	Hyperparameters of Bayesian model

Functions

$E[\cdot]$	Expectation operator
$\| \cdot \|_0$	L0-norm

number of samples, which may result in unacceptable computational costs for a large IES with large numbers of random variables.

Many new methods with reduced computational burden have been developed for the probabilistic multi-energy flow calculation of IES. These methods mainly fall into three categories: the approximation methods, analytical methods, and surrogate model methods [17]. Point estimation method is a representative approximation method that utilizes the statistical features of the input variables to describe the moments of the output variables. It has been widely applied in probabilistic multi-energy flow calculations, considering the uncertainties from multi-energy loads [18], renewable energies [19, 20], and demand response [21]. However, the point estimation method cannot directly obtain the probabilistic density function (PDF) of the output random variables, and it shows low accuracy on higher-order moments.

The semi-invariant method is the most commonly used analytical method because of its high efficiency and low computational complexity. For example, the semi-invariant method is used in the planning of distributed generation, considering the uncertainties of wind turbines and photovoltaics in [22]. The semi-invariant method and Gram–Charlier expansion are used to construct the PMEF model in [23]. However, the semi-invariant method is based on linearized energy flow equations that lead to lower accuracy. It is also difficult to effectively incorporate the correlations between different uncertainties in these semi-invariant methods.

The surrogate model method is a newly developed type of probabilistic analysis method, among which the polynomial chaos expansion method has gained popularity owing to its high efficiency and accuracy. Polynomial chaos expansion methods can be further classified into intrusive and non-intrusive methods. The intrusive methods, represented by the generalized polynomial chaos (gPC) method [24], approximate probabilistic solutions by applying expansions to differential or algebraic equations containing random input variables. Attempts have been made to apply the gPC method in the probabilistic analysis of power systems, such as probabilistic power flow calculation [25, 26] and dynamic stochastic simulation with distributed generation [27, 28].

However, in the PMEF calculation of an IES, the random variables for the multi-energy sources and loads are usually numerous and diverse. These random variables may exhibit correlations because of their shared impact factors such as ambient temperature and weather. In this situation, the gPC method suffers from two problems. First, it is still difficult for the gPC method to deal with the correlation between random variables. More complex algorithms need to be introduced to realize the processing of correlations, which significantly decreases the computational efficiency. Second, the gPC method uses polynomial bases to approximate the output responses of a system. However, the number of polynomial bases increases exponentially according to the size and type of random variables, resulting in unsolvable largescale equations, that is, the "curse of dimensionality" [29]. These problems limit the application of the gPC method to the PMEF of an IES.

In this study, a non-intrusive probabilistic multi-energy flow calculation method based on sparse polynomial chaos expansion (sPCE) is developed for the analysis of IES with massive correlated uncertainties, as shown in Fig. 1. The proposed probabilistic multi-energy flow method is further employed in the operation risk analysis of an IES to demonstrate its applicability and validity. The main contributions of this study are summarized as follows:

- An sPCE-based non-intrusive PMEF method is proposed for an IES with multiple and numerous uncertainty factors. The non-intrusive framework provides an efficient way to deal with the correlated random variables in an IES [30]. Bayesian compressive sensing (BCS) theory is employed to further reduce the dimension of the polynomial chaos expansions and effectively improve the computational efficiency.

- A quantified operation risk analysis method for an IES is developed based on the proposed PMEF calculation method. The operational risk indices for multiple energy carriers in an IES are defined. A conditional value-at-risk (CVaR) model is constructed to assess the risk index based on the probabilistic multi-energy flow calculation results. A case study based on a typical IES demonstrated the effectiveness of the proposed method.

The remainder of this paper is organized as follows. Section 2 describes the modeling method for the multi-energy flow calculation of an IES. Section 3 presents the PMEF calculation method of the IES based on sPCE and Bayesian compressive sensing theory. Section 4 establishes the risk analysis method for an IES based on the proposed probabilistic mul,ti-energy flow method. Section 5 discusses a case study that is conducted to verify the proposed method. The conclusions are presented in Section 6.

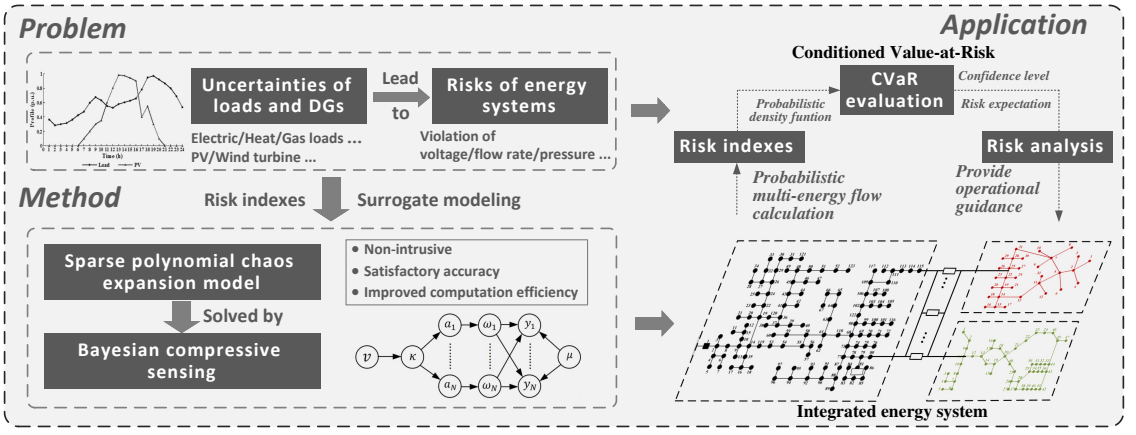

Figure 1: Framework of the proposed sPCE-based PMEF calculation method and its application

2. Modeling for the multi-energy flow calculation of IES

This section presents the multi-energy flow calculation models for the IES, including the electric network, heat network, gas network, and multi-energy station.

2.1. Modeling of the electric network

The active and reactive power flow equations for the ith electric node can be calculated as follows:

$$P_i = U_i \sum_{j \in i} U_j \left(G_{ij} \cos\left(\theta_i - \theta_j\right) + B_{ij} \sin\left(\theta_i - \theta_j\right) \right) \tag{1}$$

$$Q_i = U_i \sum_{j \in i} U_j \left(G_{ij} \sin\left(\theta_i - \theta_j\right) - B_{ij} \cos\left(\theta_i - \theta_j\right) \right) \tag{2}$$

where P_i and Q_i denote the active and reactive power injection into node i; U_i and U_j denote the voltage magnitudes of nodes i and j; G_{ij} and B_{ij} denote the real and imaginary parts of the element (i, j) in the nodal admittance matrix; and θ_i and θ_j denote the phase angles of nodes i and j, respectively.

2.2. Modeling of the heat network

The energy flow model of the heat network consists of hydraulic model and thermal model [31]. The hydraulic model describes the fluid distribution in the network according to two basic topology laws. First, the sum of mass flows that enter and leave a node must be equal to zero. Second, the sum of the head losses in a loop must be equal to zero. These two laws can be expressed as:

$$\boldsymbol{A}_{\mathrm{h}} \boldsymbol{m} - \boldsymbol{m}_{\mathrm{L}} = \boldsymbol{0} \tag{3}$$

$$\boldsymbol{B}_{\mathrm{h}} \boldsymbol{K}_{\mathrm{h}} \boldsymbol{m} |\boldsymbol{m}| = \boldsymbol{0} \tag{4}$$

where $\boldsymbol{A}_{\mathrm{h}}$ denotes the node-pipeline connection matrix of the heat network; $\boldsymbol{m}$ denotes the flow rate vector in the heat pipelines; $\boldsymbol{m}_{\mathrm{L}}$ denotes the flow rate vector of the loads; $\boldsymbol{B}_{\mathrm{h}}$ denotes the loop-branch connection matrix; and $\boldsymbol{K}_{\mathrm{h}}$ denotes the resistance coefficient matrix of the pipelines.

The thermal model contains the following equations that describe the thermal behaviors of the loads, pipelines, and thermal energy balance of the system [32].

$$W_i = C_{\mathrm{p}} m_{\mathrm{L},i} \left(T_{\mathrm{s},i} - T_{\mathrm{o},i} \right) \tag{5}$$

$$T_{\mathrm{end},k} = \left(T_{\mathrm{start},k} - T_{\mathrm{a}} \right) \exp\left(-R_k L_k / C_{\mathrm{p}} m_k \right) + T_{\mathrm{a}} \tag{6}$$

$$\left(\sum m_{\mathrm{out},k} \right) T_{\mathrm{start},k} = \sum m_{\mathrm{in},k} T_{\mathrm{end},k} \tag{7}$$

Eq. (5) illustrates the nodal heat power demanded by the heat loads, in which W_i denotes the heat load power of node i; C_{p} denotes the specific heat capacity; $m_{\mathrm{L},i}$ denotes the injected flow rate of node i; and $T_{\mathrm{s},i}$ and $T_{\mathrm{o},i}$ respectively denote the supply and output temperatures of node i. Eq. (6) indicates that the outlet temperature of a pipe can be calculated based on the temperature drop along the pipeline, where $T_{\mathrm{start},k}$ and $T_{\mathrm{end},k}$ denote the temperatures of the start and end nodes of pipeline k; T_a denotes the atmospheric temperature; R_k is the heat transfer coefficient of the pipeline k; L_k is the length of pipeline k; and m_k denotes the flow rate within pipeline k. The mixture temperature at a node with multiple incoming pipelines is calculated using Eq. (7), where $m_{\mathrm{in},k}$ and $m_{\mathrm{out},k}$ denote the flow rate of pipeline k that enters and leaves the node, respectively.

2.3. Modeling of the gas network

The model of a gas network consist of pipelines and compressors. The steady-state gas pipeline model [33] can be expressed as:

$$f_k = C_{\mathrm{g}} \frac{T_{\mathrm{n}}}{p_{\mathrm{n}}} D_k^{\frac{8}{3}} \sqrt{\frac{\left({p_i}^2 - {p_j}^2 \right)}{S L_k T Z}} \tag{8}$$

where f_k denotes the flow rate of gas pipeline k; C_{g} denotes the coefficients of the Weymouth equation; T_{n} denotes the standard temperature; p_{n} denotes the standard atmospheric pressure; p_i and p_j respectively denote the pressure of

nodes i and j; S denotes the specific gravity of gas; L_k denotes the length of the pipeline k; D_k denotes the diameter of the pipeline k; T denotes the temperature of the gas; and Z denotes the gas compressibility coefficient.

Similar with Kirchhoff's current law in electric network, the sum of gas flowing into and out of a node must be zero in the gas network. The nodal Kirchhoff's current law equations of the gas network can be expressed as follows:

$$\boldsymbol{A}_{\mathrm{g}}\boldsymbol{f} - \boldsymbol{f}_{\mathrm{L}} = \boldsymbol{0} \tag{9}$$

where $\boldsymbol{A}_{\mathrm{g}}$ denotes the node-pipeline connotation matrix; $\boldsymbol{f}$ denotes the vector of the flow rate in the pipelines; and $\boldsymbol{f}_{\mathrm{L}}$ denotes the vector of the gas flow rate injected into the nodes.

Compressors are commonly used to adjust the pressure along the pipelines. The power consumption of a compressor driven by an electric motor can be regarded as the load of the electric subnetwork. The horsepower H_{c} and consumed power P_{c} of the compressor are calculated as follows [34]:

$$H_{\mathrm{c}} = K_{\mathrm{c}} f_{\mathrm{c}} \left[\left(\frac{p_i}{p_j} \right)^{Z\frac{a-1}{a}} - 1 \right] \tag{10}$$

$$P_{\mathrm{c}} = \eta_a + \eta_b H_{\mathrm{c}} + \eta_c {H_{\mathrm{c}}}^2 \tag{11}$$

where K_{c} denotes the output coefficient; f_{c} denotes the flow rate of the compressor; a denotes the relative specific heat capacity; and η_a, η_b, and η_c denote the energy consumption coefficients of the compressor.

2.4. Unified modeling of the multi-energy station

The unified energy bus (UEB) model [35] is used to formulate the model for multi-energy stations. This unified model provides a way to incorporate different energy sources, energy conversion devices, and loads into the model of multi-energy stations. A schematic diagram of model structure is shown in Fig. 2, in which the symbols α, β, and γ denote the energy types.

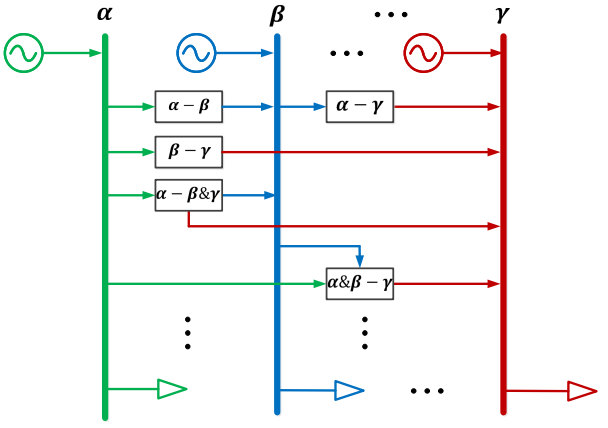

Figure 2: The unified energy bus model of integrated energy system

The model of the energy station includes energy flow, energy conversion, and load balance equations. The energy flow equations describe the energy flow balance of each energy bus, which is formulated as:

$$\sum_{i=1}^{m} F_{b,i}^{\mathrm{in}} = \sum_{j=1}^{n} F_{b,j}^{\mathrm{out}} \quad b \in \{\alpha, \beta, \gamma, \ldots\} \tag{12}$$

where $F_{b,i}^{\mathrm{in}}$ denotes the ith energy flow entering energy bus b; $F_{b,j}^{\mathrm{out}}$ denotes the jth energy flow leaving energy bus b; and m and n respectively denote the numbers of branches that enter and leave the energy bus b.

The energy conversion equation describes the coefficient of performance (COP) or efficiency of the energy conversion equipment, which is expressed as:

$$F_{e,i}^{\text{in}}\eta_{e,ij} = F_{e,j}^{\text{out}} \quad \varepsilon \in \{\alpha-\beta, \beta-\gamma, \alpha-\gamma, \dots\} \tag{13}$$

where $F_{e,i}^{\text{in}}$ and $F_{e,j}^{\text{out}}$ denote the ith input and jth output energy flow of device e; and $\eta_{e,ij}$ denotes the conversion efficiency or COP between the ith input and jth output of device e.

The load balance equation describes how the loads on an energy bus are allocated to the energy supply equipment, which is expressed as:

$$F_{b,i}^{\text{in}} = c_{b,i}L_b \quad b \in \{\alpha, \beta, \gamma, \dots\} \tag{14}$$

where L_b denotes the load of energy bus b, and $c_{b,i}$ denotes the distribution coefficient of the ith input energy flow of bus b.

Eqs. (12)–(14) can be combined according to the energy station configuration and topology, forming an energy station model expressed as a set of linear equations.

2.5. Unified multi-energy flow calculation model of IES

By combining Eqs. (1)-(14), the unified multi-energy flow model of the IES can be formulated and expressed as a nonlinear equation set as follows:

$$\boldsymbol{Y} = \boldsymbol{f}(\boldsymbol{x}) \tag{15}$$

where $\boldsymbol{Y}$ denotes the output response including the voltage magnitude, phase angle, supply temperature, and gas pressure; and $\boldsymbol{x}$ denotes the input variables including the injected active/reactive power, heat power, and gas flow rate. The Newton-Raphson method is applied to solve Eq. (15), and the iteration format can be expressed as:

$$\Delta\boldsymbol{x} = -\boldsymbol{J}^{-1}\Delta\boldsymbol{Y} \tag{16}$$

where $\Delta\boldsymbol{x}$ denotes the variation of the output variables, $\boldsymbol{J}$ denotes the Jacobian matrix, and $\Delta\boldsymbol{Y}$ denotes the variation of the input variables. The Jacobian matrix $\boldsymbol{J}$ can be formulated as:

$$\boldsymbol{J} = \begin{bmatrix} \frac{\partial\Delta\boldsymbol{P}}{\partial\boldsymbol{\theta}} & \frac{\partial\Delta\boldsymbol{P}}{\partial\boldsymbol{V}} & \frac{\partial\Delta\boldsymbol{P}}{\partial\boldsymbol{p}} & \boldsymbol{0} & \boldsymbol{0} & \boldsymbol{0} \\ \frac{\partial\Delta\boldsymbol{Q}}{\partial\boldsymbol{\theta}} & \frac{\partial\Delta\boldsymbol{Q}}{\partial\boldsymbol{V}} & \boldsymbol{0} & \boldsymbol{0} & \boldsymbol{0} & \boldsymbol{0} \\ \frac{\partial\Delta\boldsymbol{f}}{\partial\boldsymbol{\theta}} & \frac{\partial\Delta\boldsymbol{f}}{\partial\boldsymbol{V}} & \frac{\partial\Delta\boldsymbol{f}}{\partial\boldsymbol{p}} & \boldsymbol{0} & \boldsymbol{0} & \boldsymbol{0} \\ \frac{\partial\Delta\boldsymbol{f}}{\partial\boldsymbol{m}} & \boldsymbol{0} & \boldsymbol{0} & \frac{\partial\Delta\boldsymbol{W}}{\partial\boldsymbol{m}} & \frac{\partial\Delta\boldsymbol{W}}{\partial\boldsymbol{T}_{\text{s}}} & \boldsymbol{0} \\ \boldsymbol{0} & \boldsymbol{0} & \boldsymbol{0} & \frac{\partial\Delta\boldsymbol{T}_{\text{s}}}{\partial\boldsymbol{m}} & \frac{\partial\Delta\boldsymbol{T}_{\text{s}}}{\partial\boldsymbol{T}_{\text{s}}} & \boldsymbol{0} \\ \boldsymbol{0} & \boldsymbol{0} & \boldsymbol{0} & \frac{\partial\Delta\boldsymbol{T}_{\text{r}}}{\partial\boldsymbol{m}} & \boldsymbol{0} & \frac{\partial\Delta\boldsymbol{T}_{\text{r}}}{\partial\boldsymbol{T}_{\text{r}}} \end{bmatrix} \tag{17}$$

In scenarios with uncertainties, $\boldsymbol{x}$ in Eq. (15) is transformed from a deterministic input variable to a stochastic input variable and $\boldsymbol{Y}$ consequently becomes a stochastic output response, forming the PMEF problem of the IES. This problem can be solved using many statistical methods such as the commonly used MCS. In this study, the following PMEF calculation method is proposed for Eq. (15) to improve the overall solving performance.

3. Structure for PMEF calculation of IES

In this section, a PMEF calculation method is proposed for IES. First, the Gaussian-Copula function is employed to describe the correlations among the random variables. Subsequently, the sparse polynomial chaos expansion (sPCE) structure for the PMEF calculation of the IES is developed. Finally, a sparse surrogate model is constructed using the Bayesian compressive sensing (BCS) method to efficiently obtain the probabilistic distribution of the IES operation states.

3.1. Handling of the correlated random variables in the IES

The renewable energy sources and loads in an IES generally exhibit diverse uncertainties, which have been extensively studied in existing literature. In this study, the normal, Beta, and Weibull distributions are used to describe the uncertainties in loads, PV, and wind generation, respectively. Moreover, owing to common factors such as weather, temperature, and users' energy usage habits, there are correlations between these uncertainties. Assuming u and v are two random input variables in the PMEF problem, the Copula theory is employed to handle their correlations, which can be expressed as:

$$C(u,v)=\int_{-\infty}^{\Phi^{-1}(u)}\int_{-\infty}^{\Phi^{-1}(v)}\frac{1}{2\pi\sqrt{1-\rho^2}}e^{\frac{s^2-2\rho st+t^2}{2\left(1-\rho^2\right)}}\,\mathrm{d}s\,\mathrm{d}t \tag{18}$$

where $\Phi^{-1}(u)$ and $\Phi^{-1}(v)$ are the inverse functions of standard normal distribution, and ρ denotes the linear correlation coefficient. Based on the Gaussian-Copula function, the joint PDF can be obtained by combining the marginal distributions u and v of the random variables and their rank correlation coefficients ρ [36]. The sampling process can be performed according to the joint PDF to generate samples with random decorrelated input variables.

3.2. Polynomial chaos expansion for PMEF calculation

After decorrelation, $\boldsymbol{x}$ becomes an n-dimensional random vector with independent components in the probabilistic multi-energy flow stochastic function $\boldsymbol{y}=\boldsymbol{f}(\boldsymbol{x})$. According to polynomial chaos expansion (PCE) theory [24], response y can be approximated using a multidimensional polynomial chaos expansion model $P(\boldsymbol{x})$ as:

$$y=f(\boldsymbol{x})\approx P(\boldsymbol{x})=\sum_i a_i\Phi_i(x) \tag{19}$$

where $x=[x_1,x_2,\ldots,x_n]$ denotes an n-dimensional independent random vector; $\Phi_i(x)$ denotes the orthogonal polynomial basis; a_i denotes expansion coefficients; $P(\boldsymbol{x})$ denotes the polynomial approximation of the original PMEF model and can be utilized as a surrogate model for efficient multi-energy flow calculations; and $\Phi_i(x)$ denotes the polynomial basis, that should satisfy the following orthogonality condition:

$$E\left[\Phi_i(x)\Phi_j(x)\right]=\int\Phi_i(x)\Phi_j(x)\omega(x)\mathrm{d}x=\begin{cases}0 & i=j\\ E\left[\phi_i^2(x)\right] & i\neq j\end{cases} \tag{20}$$

where $E[\cdot]$ denotes the expectation operator, and $\omega(x)$ denotes the weight function.

An orthogonal polynomial basis can be selected according to the distribution of variables. Some typical probability distribution functions and their corresponding polynomials, also known as the Wiener-Askey scheme of orthogonal polynomials [37], as listed in Table 1.

Table 1
Wiener-Askey scheme of orthogonal polynomials

Variable	Distribution	Orthogonal polynomial	Weight function
Load	Gaussian	Hermite	$\frac{1}{\sqrt{2\pi}}e^{-x^2/2}$
Photovoltaic	Beta	Jacobi	$(1-x)^{\alpha}(1+x)^{\beta}$

The orthogonal polynomial basis of the Weibull distribution associated with a wind turbine is constructed using the discretized Stieltjes procedure [38]. Then, the set of polynomial bases $\boldsymbol{\phi}$ can be obtained for each independent variable, which is expressed as:

$$\boldsymbol{\phi}=\left\{\phi_i^j\left(x_i\right)\right\}\quad i=1,2,\ldots,n;j=1,2,\ldots,r \tag{21}$$

where $\phi_i^j(x_i)$ denotes the jth basis of the ith random variable x_i; n denotes the number of variables; and r denotes the highest expansion order.

Note that $\boldsymbol{\phi}$ is the basis of the random input variable rather than that of the response function. Thus, for all the n random variables, there will exist $r\times n$ bases in total. The ith polynomial basis $\phi_i(\boldsymbol{x})$ of the response function can then be calculated using:

$$\Phi_i(\boldsymbol{x})=\prod_{i=1}^{n}\phi_i^{(k_i)}\left(x_i\right) \tag{22}$$

where k_i satisfies $0 \le \sum_{i=1}^{n} k_n \le r$, indicating that the highest order of the basis cannot exceed r.

After selecting the optimal basis polynomials, expansion coefficient a_i should be calculated to obtain the surrogate model. The least squares method is used to calculate the coefficients based on the sampling data. The sampling process is also known as the experimental design, which samples the random input variables and conducts a calculation for each scenario. Thus, the problem is transformed into the following residual minimization problem:

$$\hat{\boldsymbol{a}} = \operatorname{argmin} \sum_{i=1}^{N} \left[y^{\mathrm{ED}}\left(x^{(i)}\right) - a^{\mathrm{T}}\Phi\left(x^{(i)}\right)\right]^2 \tag{23}$$

where N denotes the experimental design size; $x^{(i)}$ denotes the ith sampling data set of the random variables; and y^{ED} denotes the experimental design of the target response Y of the original multi-energy flow model. Once the coefficients have been determined, the polynomial chaos expansion of the response is derived.

3.3. Sparse coefficients calculation based on Bayesian compressive sensing

As indicated in Eq.(22), the number of expansion terms in the full PCE model can reach $M = (r+n)!/(r!n!)$. To ensure expansion accuracy, the size of the experimental design is typically set to $N = 2M$ [17]. Under this condition, as the expansion order r or the number of variables n increases, the number of coefficients M and the size of the experimental design N increase rapidly, which significantly limit the calculation efficiency.

However, in the PMEF of the IES, most coefficients of the high order expansion terms tend to be zero and can be ignored. The sensitivity of the response to each input variable is also different. For example, electric load fluctuations usually impact the nearby bus voltage more than the far-away ones. The coefficients of the less influential expansion terms can also be considered zero to reduce the computational burden. Therefore, the PCE-based probabilistic multi-energy flow model can be considered sparse. Eq. (23) is then transformed into the problem of minimizing the number of non-zero elements in the coefficient vector a:

$$\begin{cases} \hat{\boldsymbol{a}} = \operatorname{argmin} \|\boldsymbol{a}\|_0 \\ \text{s.t.} \quad \boldsymbol{y}^{\mathrm{ED}} - \boldsymbol{a}^{\mathrm{T}}\boldsymbol{\Phi} = \boldsymbol{0} \end{cases} \tag{24}$$

where $\|\boldsymbol{a}\|_0$ denotes L0 norm.

The Bayesian compressive sensing method [39] is applied to solve Eq. (24) for the expansion coefficients $\hat{a}$. The idea of the BCS method is to select the polynomial basis function that is the most relevant to the residual vector according the correlation function in each step, which is given as follows:

For a given orthogonal polynomial basis and initial experimental design, the likelihood function is given as follows:

$$P(\boldsymbol{Y}|\boldsymbol{\Phi}, \boldsymbol{a}, \mu) = N\left(\boldsymbol{Y}|\boldsymbol{a}\boldsymbol{\Phi}, \mu^{-1}\right) \tag{25}$$

where the likelihood function follows a Gaussian distribution with a variance of μ^{-1}.

The problem in Eq. (24) is equivalent to applying a Laplace prior on the coefficients a. Hence, hierarchical priors are applied to deal with this problem [40].

$$P(\boldsymbol{a}|\lambda) = \prod_{i=1}^{P} N\left(c_i|0, \lambda_i\right) \tag{26}$$

$$P\left(\lambda_i|\kappa\right) = \Gamma\left(\lambda_i|1, \frac{\kappa}{2}\right) = \frac{\kappa}{2}\exp\left(-\frac{\kappa\lambda_i}{2}\right) \tag{27}$$

Thus, the posterior distribution of all parameters can be obtained by using the Bayesian inference:

$$P(\boldsymbol{a}, \lambda, \kappa, \mu|\boldsymbol{y}) = \frac{P(\boldsymbol{y}|\boldsymbol{a}, \mu)P(a|\lambda)P(\lambda|\kappa)P(\mu)P(\kappa)}{P(\boldsymbol{y})} \tag{28}$$

The dependencies of the hyper parameters in joint probability model are shown in Fig. 3.

Thus, the posterior distribution of a can be obtained from $P(\boldsymbol{a}, \lambda, \kappa, \mu|\boldsymbol{y})$. It follows a Gaussian distribution $N(\boldsymbol{a}|\mu_a, \Sigma_a)$ with:

$$\delta_a = \Sigma_c \mu \boldsymbol{\Phi}^{\mathrm{T}}\boldsymbol{y} \tag{29}$$

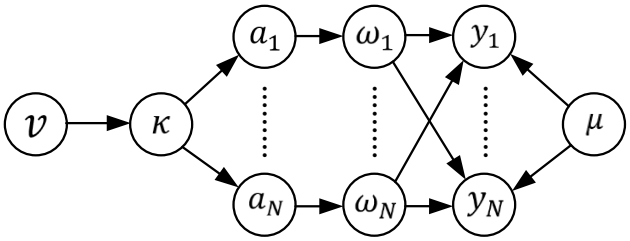

Figure 3: Graphical model representing the Bayesian model parameters

$$\Sigma_a = \left(\mu \mathbf{\Phi}^{\mathrm{T}} \mathbf{\Phi} + \mathrm{diag}\left(\frac{1}{\lambda_i} \right) \right)^{-1} \tag{30}$$

Therefore, the hyper parameters in Eqs. (29) and (30) can be calculated by maximizing $P(\boldsymbol{y}, \boldsymbol{\lambda}, \kappa, \mu)$. A fast Laplace algorithm is applied to reduce the computational cost by updating a single λ_i rather than total λ in each step. Thus, the update of δ_c and Σ_c could become more efficient. We refer to [41] for the further details of the algorithm.

4. PMEF-based operation risk analysis of IES

The PMEF calculation method could efficiently obtain the probabilistic distribution of energy flows, which is essential for the operational risk analysis of an IES. In this section, the risk index in the IES is introduced. Subsequently, the CVaR model is constructed to perform a probabilistic analysis of the operation risk. Finally, the framework of the probabilistic multi-energy flow based risk analysis of an IES is established.

4.1. Indices for risk analysis of IES

4.1.1. Voltage violation in electric networks

The voltage quality is a critical index for the operation of electric networks. The nodal voltage in an electric network must be limited within a certain range. The average violation voltage value of all the nodes is chosen to quantify the voltage risk for the electric network, which can be expressed as:

$$\delta_{\mathrm{E}}(i) = \begin{cases} \left(V_i - V_{i,\max}\right)/V_{\mathrm{b},i} & V_i > V_{i,\max} \\ \left(V_{i,\min} - V_i\right)/V_{\mathrm{b},i} & V_i < V_{i,\min} \\ 0 & V_{i,\min} \le V_i \le V_{i,\max} \end{cases} \tag{31}$$

$$f_{\delta \mathrm{E}} = \frac{1}{n_{\mathrm{E}}} \sum_{i=1}^{n_{\mathrm{E}}} \delta_{\mathrm{E}}(i) \tag{32}$$

where $\delta_{\mathrm{E}}(i)$ denotes the voltage violation index of node i; $V_{i,\max}$ denotes the upper limit of the voltage magnitude of node i; $V_{i,\min}$ denotes the lower limit of the voltage magnitude of node i; $V_{b,i}$ denotes the basic voltage magnitude of node i; $f_{\delta \mathrm{E}}$ denotes the voltage violation index of the electric subsystem; and n_{E} denotes the number of nodes in the electric subsystem. The basic voltage magnitude is typically set to the rated value, that is, 1.0 p.u. when the electric load flow is calculated in per-unit value. The upper limit $V_{i,\max}$ is set to 1.05 p.u. and the lower limit $V_{i,\min}$ is set to 0.95 p.u. in this study.

4.1.2. Flow rate violation in heat networks

Flow rate violation is considered to be the main risk in the operation of a heat network. Therefore, the average violation flow rate value of pipelines is defined as the risk index of the heat network [42], which can be expressed as:

$$\delta_{\mathrm{H}}(k) = \begin{cases} \left(m_k - m_{k,\max}\right)/m_{k,\max} & m_k > m_{k,\max} \\ 0 & m_k \le m_{k,\max} \end{cases} \tag{33}$$

$$f_{\delta \mathrm{H}} = \frac{1}{n_{\mathrm{H}}} \sum_{k=1}^{n_{\mathrm{H}}} \delta_{\mathrm{H}}(k) \tag{34}$$

where $\delta_{\mathrm{H}}(k)$ denotes the flow rate violation index of pipeline k; $m_{k,\max}$ denotes the upper limit of the flow rate of pipeline k; $f_{\delta\mathrm{H}}$ denotes the flow rate violation index of the heat subsystem; and n_{H} denotes the number of pipelines in the heat subsystem.

4.1.3. Pressure violation in gas networks

The nodal pressure in a gas network must be limited to a certain range to guarantee operational security. Therefore, the average violation pressure value of all the nodes is defined to describe the risk in the gas networks, which can be calculated using:

$$\delta_{\mathrm{G}}(i)=\begin{cases}\left(p_i-p_{i,\max}\right)/p_{\mathrm{b},i} & p_i>p_{i,\max}\\ \left(p_{i,\min}-p_i\right)/p_{\mathrm{b},i} & p_i<p_{i,\min}\\ 0 & p_{i,\min}\le p_i\le p_{i,\max}\end{cases} \tag{35}$$

$$f_{\delta\mathrm{G}}=\frac{1}{n_{\mathrm{G}}}\sum_{i=1}^{n_{\mathrm{G}}}\delta_{\mathrm{G}}(i) \tag{36}$$

where $\delta_{\mathrm{G}}(i)$ denotes the pressure violation index of node i; $p_{i,\min}$ denotes the lower limit of the pressure of node i; $p_{i,max}$ denotes the upper limit of the pressure of node i; p_b denotes the basic pressure of node i; $f_{\delta\mathrm{G}}$ denotes the pressure violation index of the gas subsystem; and n_{G} denotes the number of nodes in the gas subsystem.

4.2. Conditional Value-at-Risk for risk analysis

The PDFs of all three indices could be directly solved as the target response in the probabilistic multi-energy flow calculation, because the nodal voltage, flow rate and nodal pressure are all random state variables. Then, CVaR is applied to quantify the operational risks based on the PDF results. The concept of CVaR is developed from the Value-at-Risk (VaR) assessment model and has been widely used in the risk assessment of financial markets and power systems [43].

To construct the CVaR model, VaR is firstly defined, which represents the maximum possible loss value expected from an investment at a given confidence level and can be expressed as:

$$\mathrm{VaR}_{\beta}=\min\left\{\alpha\in R,\int_{f(x,y)\le\alpha}\rho(y)\mathrm{d}y\ge\beta\right\} \tag{37}$$

where $f(x, y)$ denotes the loss function, $\rho(y)$ denotes the probabilistic density function, β denotes the confidence level.

However, VaR cannot accurately assess the tail risk or consider extreme scenarios, which leads to lower accuracy in risk assessment. To effectively reflect the average loss of tail risk, CVaR is used to describe the expected value of the risk exceeding VaR under a given confidence level.

The value of CVaR can be calculated using:

$$\mathrm{CVaR}_{\beta}=\alpha+\frac{1}{N(1-\beta)}\sum_{i=1}^{N}\left[f_{\delta}-\alpha\right]^{+} \tag{38}$$

where α denotes the value of VaR; N denotes the number of samples; and $[f_{\delta}-\alpha]^{+}$ denotes the maximum value between $f_{\delta}-\alpha$ and 0.

4.3. Procedure of PMEF-based risk analysis of IES

The structure of the PMEF-based risk assessment of the IES proposed in this study is shown in Fig. 4, and its detailed steps are summarized as follows:

Step 1): Input deterministic and random parameters of the IES. The deterministic parameters included those of the multi-energy networks and energy stations. The random parameters included the PDFs of the loads, output power of the distributed generators, and correlation coefficients between random variables.

Step 2): Establish a multi-energy flow model based on the deterministic input parameters.

Step 3): Establish the Gaussian-Copula function of the correlated random variables $\boldsymbol{X}$ according to their correlation coefficients. Then, the sample from the joint PDF $\boldsymbol{X}$ to generates a decorrelated dataset $\boldsymbol{x}_{\mathrm{ED}}$ of random variable $\boldsymbol{X}$.

Step 4): Perform deterministic multi-energy flow calculation of IES to gain the samplings of target output response

$\boldsymbol{y}_{\mathrm{ED}}$.

Step 5): Determine the orthogonal polynomial bases according to the predefined types of input variables. Use the sampling data $\boldsymbol{x}_{\mathrm{ED}}$ and response $\boldsymbol{y}_{\mathrm{ED}}$ to estimate the sparse coefficients of the bases using the BCS method. Thus, a surrogate model for the selected response can be established.

Step 6): Sample the random variable $\boldsymbol{X}$ and calculate the response of each sample. Then the curves of the PDFs of the selected responses, including nodal voltages, flow rates in the heat pipelines, and pressures of the gas nodes, can be obtained from the statistical results of all samples.

Step 7): Calculate the CVaR values of the risk indices according to the sampling data. Then the CVaR value of the risk indices can be employed in operational risk analysis.

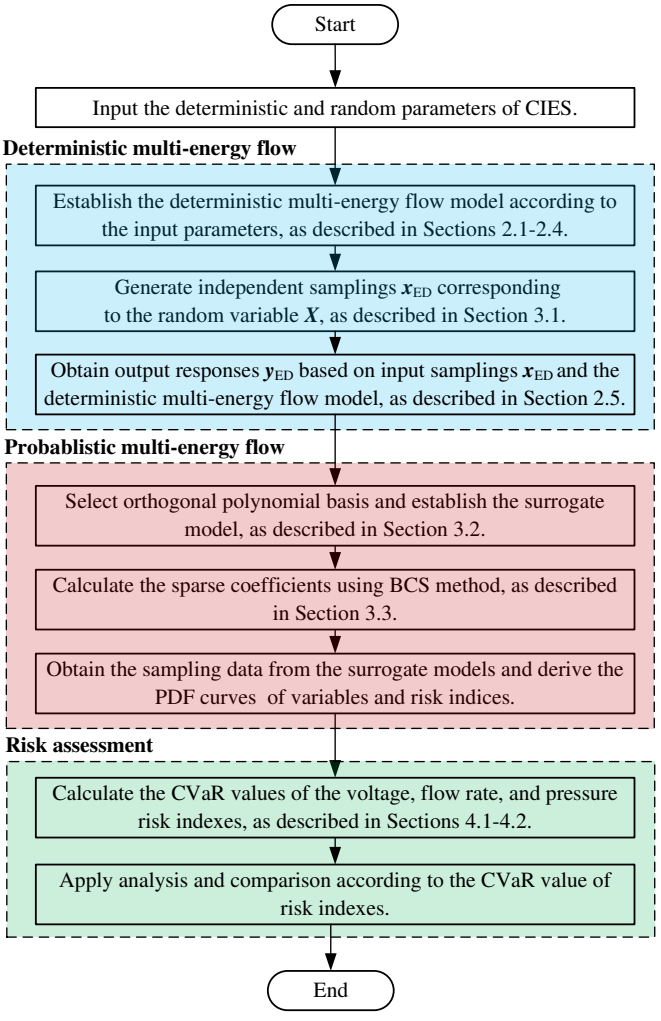

Figure 4: Flowchart of the PMEF based risk analysis method

5. Results and discussions

5.1. Case study

The structure of the IES in this case study is shown in Fig. 5, in which the IEEE 123-node distribution network [44], 32-node heat network [31] and 48-node gas network [45] are coupled through four energy stations. The configurations of the energy stations are listed in Table 2. In this study, it is assumed that the electric, heat, and gas loads follow a Gaussian distribution [46], and the output power of the PV and wind turbine follows the Beta [47] and Weibull

distributions [48], respectively. The types of random variables in each energy subsystem are listed in Table 3. The correlation coefficients among random variables are listed in Table 4, where the subscripts e, h, g, p, and w denote electricity, heat, gas, PV, and wind turbine, respectively. The proposed method is implemented using MATLAB R2018a on a computer with an Intel Core i5-8500 3.00GHz CPU and 8 GB memory.

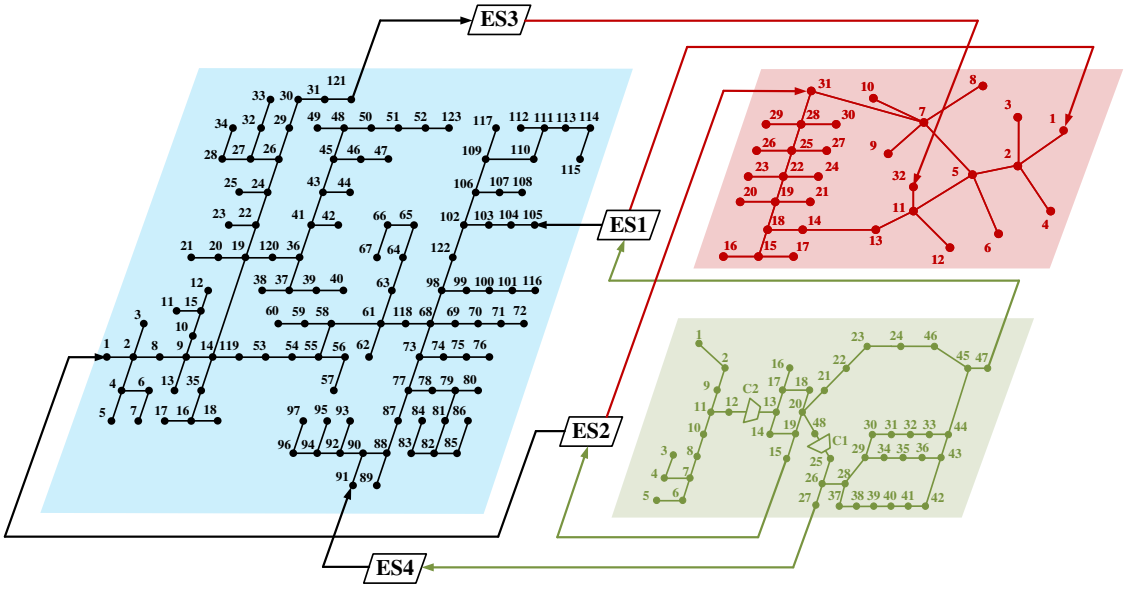

Figure 5: The structure of the test IES consists of an electric network (blue), a heat network (red), a gas network (green), and 4 energy stations

Table 2
Configuration of the energy stations

Energy Station	Configuration	Electricity node	Heat node	Gas node
ES1	CHP (as heat slack node)	105	1	47
ES2	CHP (as electric slack node)	1	31	15
ES3	electric boiler	121	32	-
ES4	gas turbine	91	-	27
C1	electric compressor	47	-	25
C2	electric compressor	62	-	13

Table 3
Types of uncertainties in IES

Uncertainty	Number	Type
Wind turbine	5	Weibull
Photovoltaics	5	Beta
Electric load	20	Gaussian
Heat load	10	Gaussian
Gas load	10	Gaussian

5.2. Verification of the proposed PMEF calculation method

In this section, the proposed sPCE-based probabilistic multi-energy flow method is applied to verify its accuracy and effectiveness. The modelling method of the IES is introduced in Section 2. The proposed PMEF method is

Table 4
Correlation coefficients of random variables in IES

correlation coefficient	ρ_{ee}	ρ_{hh}	ρ_{gg}	ρ_{pp}	ρ_{ww}	ρ_{ge}	ρ_{he}
	0.5	0.5	0.5	0.5	0.5	0.2	0.2

conducted according to Section 3. The proposed method is compared with two other algorithms to verify its correctness and effectiveness, as follows:

- The Monte-Carlo simulation method based on Latin hypercube sampling. The MCS method adopts 10,000 samples to obtain the PDF of the response, which is then utilized as the benchmark for comparison.
- The gPC method based on intrusive computing framework [25]. In this study, the coefficients in gPC are solved using the stochastic Galerkin method, as shown in Appendix A. The gPC method uses a 2nd order expansion, which is denoted as gPC-2.
- The proposed sparse polynomial chaos expansion method based on the Bayesian compressive sensing. The expansion order is set to two (denoted as sPCE-BCS-2) and five (denoted as sPCE-BCS-5). The sample size of experimental design is set to 300.

Note that the input correlations of MCS and sPCE are preprocessed with Gaussian-Copula functions introduced in Section 3.1, and that of gPC is preprocessed with Nataf transformation shown in Appendix B.

Taking the voltage magnitude of electric node 95, flow rate of heat pipeline 4, and pressure of gas node 10 as examples, the PDFs obtained using the MCS, gPC, and sPCE-BCS-5 methods are presented in Fig. 6. The PDFs derived by the surrogate model methods, including gPC and sPCE-BCS-5, are both calculated based on 300 samples. Compared to MCS, both gPC and sPCE could obtain results with acceptable accuracy. Based on the calculation results of the probabilistic multi-energy flow, the risk of violation can be assessed for nodes or pipelines in the energy subsystems. As shown in Fig. 6(b) and 6(d), electric node 95 has a probability of 38.38% exceeding the lower voltage limit of 0.95 p.u., and heat pipeline 4 has a probability of 2.52% exceeding its flow rate limit.

The maximum mean errors of the operational state variables in the IES are listed in Table 5. Both the gPC and sPCE-BCS methods achieved high accuracy, with most of the relative errors being smaller than 0.5%. Moreover, using the same order of polynomial expansion, gPC-2 showd a higher accuracy than sPCE-BCS-2 because of its intrusive calculation structure. However, when the expansion order of sPCE-BCS reach the 5th order, sPCE-BCS-5 overall showed a better accuracy than gPC-2.

Table 5
Maximum errors of different methods compared with Monte-Carlo method

Subsystems	Variable	$\epsilon_{\text{gPC}-2}/\%$	$\epsilon_{\text{sPCE}-\text{BCS}-2}/\%$	$\epsilon_{\text{sPCE}-\text{BCS}-5}/\%$
Electric	Voltage magnitude	0.0548%	0.1659%	0.0316%
	Phase angle	0.2337%	0.2565%	0.1574%
	Active power	-0.1247%	0.5199%	0.1606%
	Reactive power	-0.2337%	-0.2864%	-0.0753%
Heat	Flow rate	0.0109%	-0.2195%	-0.0774%
	Supply temperature	-0.3450%	0.4415%	0.0101%
	Return temperature	0.2124%	-0.1869%	-0.0891%
Gas	Pressure	-0.2742%	-0.4450%	-0.1252%
	Flow rate	0.1869%	0.3623%	0.1368%

Table 6 shows the comparison results of the computational times of the four methods. The sPCE-BCS method achieved a significant efficiency advantage over the MCS. This improvement is mainly because the sampling size is reduced by 97% in the sPCE-BCS methods. Because the multi-energy flow calculation must be repeated for each sample, a small sampling size directly leads to a reduced time cost. Although the gPC-2 method adopts the same

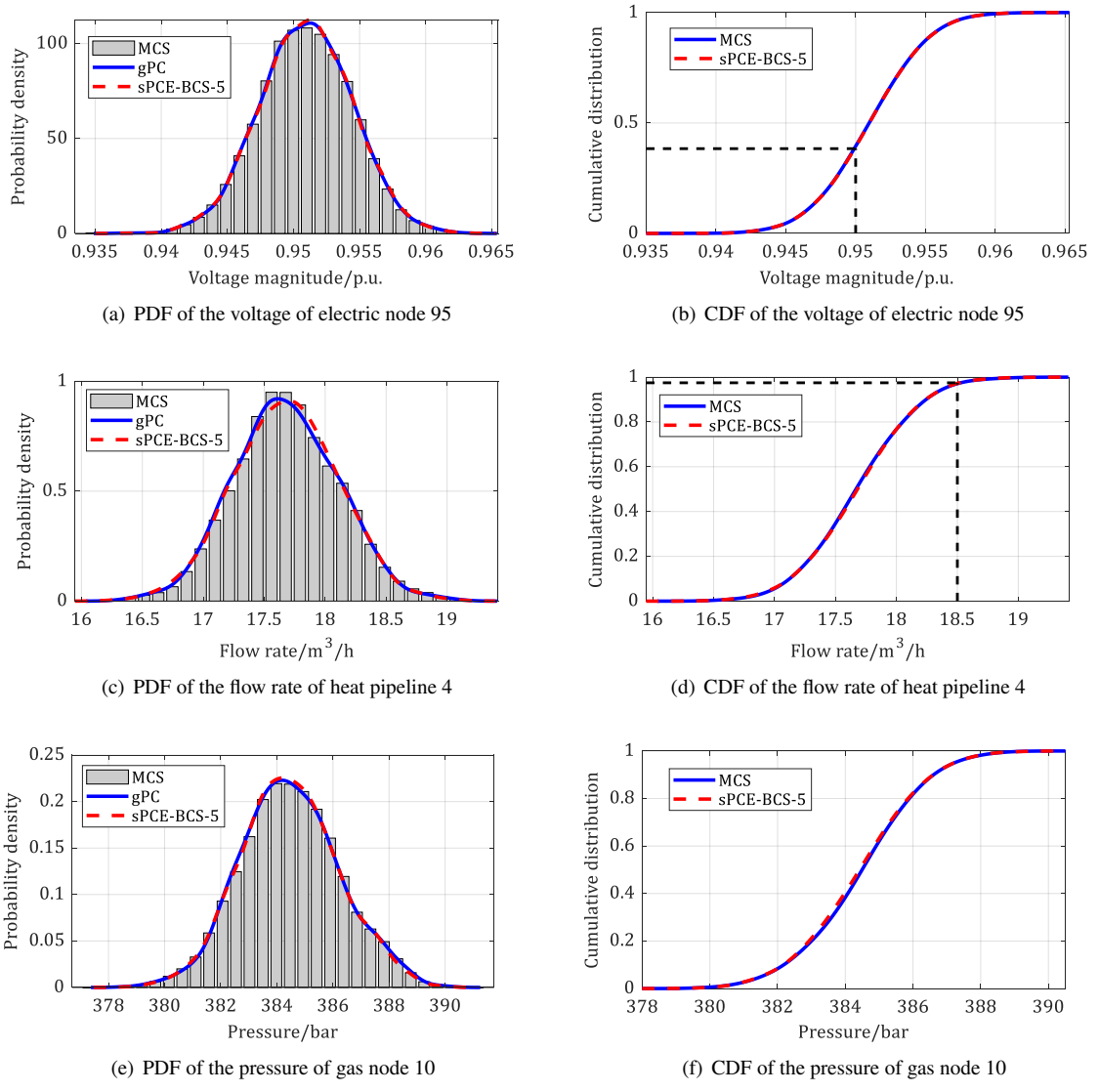

(a) PDF of the voltage of electric node 95

(b) CDF of the voltage of electric node 95

(c) PDF of the flow rate of heat pipeline 4

(d) CDF of the flow rate of heat pipeline 4

(e) PDF of the pressure of gas node 10

(f) CDF of the pressure of gas node 10

Figure 6: Comparison of the PDFs and CDFs of the state variables in the IES

sampling size, its computation time is nearly five times of the sPCE-BCS-2 and four times of the sPCE-BCS-5 method because the problem size to be solved using the gPC method increases exponentially with the size of random variables. This comparison verified the efficiency advantage of the proposed sPCE-BCS method.

The above results show that the proposed sPCE-BCS can obtain probabilistic multi-energy flow results with a substantially higher computational speed and accuracy. Although gPC-2 shows a higher accuracy than sPCE-BCS-2 for the same expansion order, sPCE-BCS can improve its accuracy by applying a higher expansion order, for example, sPCE-BCS-5, while maintaining its computation speed to be faster than the gPC method.

5.3. Application in the risk analysis of IES

In this section, the CVaR-based risk analysis method which is introduced in Section 4 is applied to the test IES case. The indices introduced in Section 4.1 are selected as the responses of the PMEF calculation. The CVaR value is calculated according to the methods introduced in Section 4.2 based on the PDF of the indices.

1) Risk analysis of single subsystem considering uncertainties of sources and loads.

Table 6
Comparison of the total calculation time using different methods

Method	Total/s
MCS	2864.1
gPC-2	480.4
sPCE-BCS-2	97.3
sPCE-BCS-5	110.7

The CVaR analysis of a single energy subsystem can be utilized to quantify the operational risks under different uncertainties, providing an essential reference to guide its interaction with other energy subsystems. In this section, the output power of DGs in the electric subsystem and loads in the heat network is considered to be increased with a proportion from 0% to 50%, which would lead a violation risk to the corresponding subsystems. The CVaR of the electric and heat subsystems is calculated to evaluate the risk index under different increasing levels of DGs and heat loads, as shown in Fig. 7.

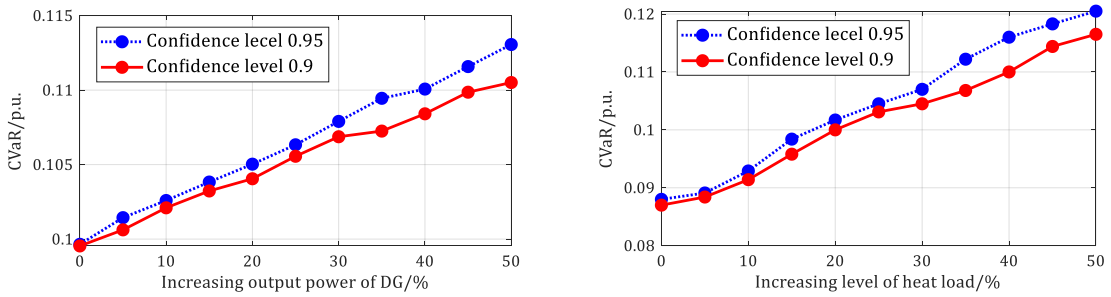

(a) Electric subsystem (b) Heat subsystem

Figure 7: CVaR values of electric and heat subnetworks under different increasing levels of DGs and heat loads

Take the results of the electric subnetwork in Fig. 7(a) as an example. For a confidence level of 0.9, the VaR and CVaR values of the risk index for the electric subnetwork are 0.085 and 0.099 p.u, respectively, when the output power of DGs is not increased. This means, for the top 10% of the most severe scenarios, the voltage violation indices have an average of 0.085 p.u. and an expectation of 0.099 p.u. With the increase of DGs' output power, the CVaR value also increases, indicating that the operation of the electric subsystem affords more risks. As the output power of DGs increases by a proportion from 0% to 50%, the CVaR value increases from 0.099 p.u. to 0.1130 p.u., indicating a rise in risk owing to changes in operation strategy. In addition, a higher confidence level produces a larger CVaR value, which means a more conservative assessment result.

2) Risk analysis of IES considering interactions between subsystems

It is assumed that the EB adjusts its output power to help consume the fluctuating renewable energy. The CHPs also need to adjust their output power to maintain the balance between the supply and demand in the IES. Uncertainties in the source and load are transmitted among the three subsystems of electricity, gas, and heat, causing risks and changes in the system operating state. The CVaR values of each energy subsystem and the overall IES are obtained.

As shown in Fig. 8, when the output power of EB is raised up to accommodate more renewable energy, the CVaR of the heat subsystem increases. Meanwhile, the CVaR of the electric subsystem decreases. The CVaR of the gas subsystem shows a smooth growth owing to the changes in the output power of the energy stations. Moreover, it can be found that the CVaR of the overall IES decreases as the accommodation level increases, which proves the benefit of interactions among multiple energy carriers.

3) Risk analysis of IES considering different operation strategies

The CVaR value of the risk indices can be used to compare and analyze the risks under different operation strategies, which is a useful guidance for the decision makers. Taking the heat subsystem as an example, ES1 works as the slack

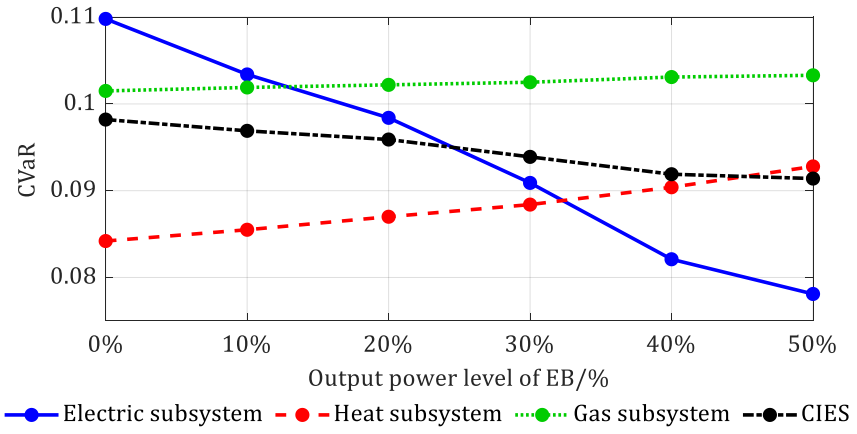

Figure 8: CVaR values of energy subsystems and IES under different output power levels of EB

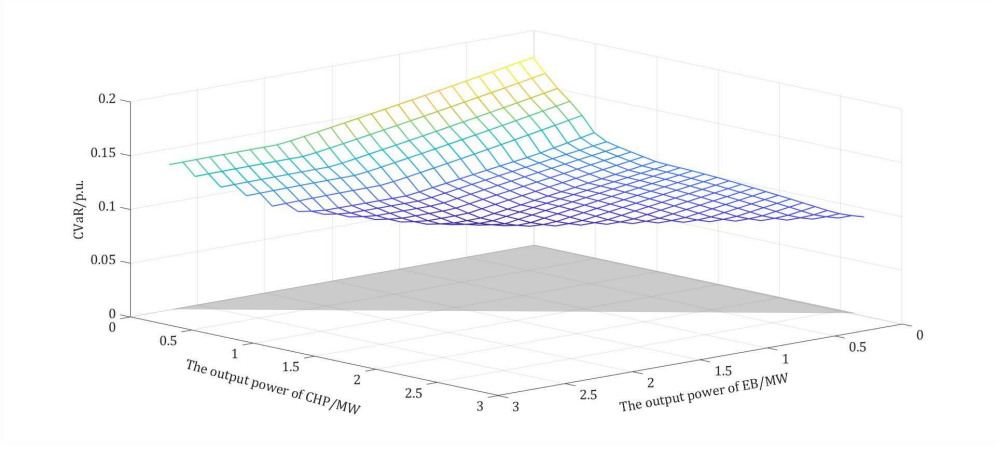

Figure 9: CVaR values of heat subsystem under different operation strategies

source. The output power of the CHP in ES2 and the EB in ES3 are determined according to the operation strategies of heat network. The CVaR value of the risk indices is shown in Fig. 9.

As shown in Fig. 9, the sum of the output power of the CHP and EB is always maintained less than the load demand, that is, 2.8 MW. The CVaR reaches its maximum value when all the load demand is supplied by the slack source, which brings severe flow rate violation risks to the pipelines near ES1. The minimum CVaR value occurs when the output power of CHP is 1.3 MW and that of the EB is 1.4 MW. The relatively balanced output of the three sources at this point results in an even distribution of the flows, which reduces the risk of flow rate violation..

6. Conclusion

In this paper, a non-intrusive probabilistic multi-energy flow calculation method is presented, and its application in the operation risk analysis of an IES is explored. Considering the correlated random variables, the proposed sPCE-BCS method can effectively calculate the probabilistic multi-energy flow and obtain the probabilistic features of the selected output response. The proposed method with different orders is compared with the MCS and gPC methods, which proved its correctness and accuracy. Moreover, the sPCE-BCS method with a higher order has a significantly higher calculation speed of probabilistic multi-energy flow with a higher accuracy compared with other methods, where sPCE-BCS-5 requires 96% less computation time than the MCS method, and 76.9% less than that of the gPC method.

The CVaR-based risk analysis is further applied to the probabilistic multi-energy flow calculation of the IES to realize the risk analysis. The results demonstrate that the risks of each energy subsystem as well as the overall IES can be effectively obtained for a quantified analysis. The calculation results also provide a reference for the secure dispatch of energy subsystems and are useful for facilitating the interactions in the IES.

In future research, a data-driven arbitrary sPCE method could be considered. The sPCE method proposed in this study needs to design probabilistic density functions for all random input variables, which cannot be realized in actual applications. Relying on large amounts of real operation data, the data-driven sPCE method can eliminate the dependence on a specific distribution and make the calculation results more realistic, which is promising for further study.

Appendix A

Let $f(Z)$ be a scalar function of a random variable Z, then the N-order gPC expansion of $f(Z)$ is defined as:

$$f(Z) \approx f_N(Z) = \sum_{i=0}^{N} f_i \Phi_i(Z) \tag{A1}$$

where $\Phi_i(Z)$ is the orthogonal polynomial basis function and satisfies:

$$E\left[\Phi_i(Z)\Phi_j(Z)\right] = \gamma_i \delta_{ij} \tag{A2}$$

With (A1) and (A2), the gPC expansion coefficient f_i can be derived as follows:

$$f_i = \frac{1}{\gamma_i} E\left[f(Z)\Phi_i(Z)\right] \tag{A3}$$

Consider the following stochastic nonlinear scalar equation:

$$g(x, p(Z)) = 0 \tag{A4}$$

where x is an unknown random variable, Z is an independent random variable with known distribution, and $p(Z)$ is a known input function. With a properly chosen basis $\Phi_k(Z)$, the N-order gPC expansions of x and $p(Z)$ can be written as:

$$x(Z) = \sum_{k=0}^{N} x_k \Phi_k(Z) \tag{A5}$$

$$p(Z) = \sum_{k=0}^{N} p_k \Phi_k(Z) \tag{A6}$$

where x_k and p_k are the expansion coefficients. Because $p(Z)$ is known, p_k can be directly obtained by using (A3). By substituting (A5) and (A6) into (A4) and projecting the equation onto each basis $\Phi_m(Z)$ (m=0,1,2,…,N), we have:

$$E\left[g\left(\sum_{k=0}^{N} x_k \Phi_k(Z), \sum_{k=0}^{N} p_k \Phi_k(Z)\right)\right] = 0 \tag{A7}$$

After evaluation of the expectation, Z disappears and $N+1$ deterministic equations are formed. Meanwhile, the unknown random variable has been transformed into $N+1$ unknown coefficients x_k. Then Newton-Raphson method can be used to solve the equations for x_k.

Appendix B

Let $\boldsymbol{C_Y}$ be the correlations matrix of the input random variables $\boldsymbol{Y} = [Y_1, Y_2, \ldots, Y_n]^{\mathrm{T}}$

$$\boldsymbol{C_Y} = \begin{bmatrix} 1 & \rho_{12} & \cdots & \rho_{1n} \\ \rho_{21} & 1 & \cdots & \rho_{2n} \\ \vdots & \vdots & \vdots & \\ \rho_{n1} & \rho_{n2} & \cdots & 1 \end{bmatrix} \tag{A8}$$

The standard normal random variables $\boldsymbol{\xi} = [\xi_1, \xi_2, \dots, \xi_n]^{\mathrm{T}}$ are introduced which satisfy:

$$\xi_k = \Phi^{-1}\left(F_k\left(Y_k\right)\right) \tag{A9}$$

where F_k is the CDF of Y_k, and $\Phi(\cdot)$ is the CDF of ξ_k. Let $\boldsymbol{C}_\xi$ be the correlation coefficient matrix of ξ.

$$\boldsymbol{C}_\xi = \begin{bmatrix} 1 & \rho'_{12} & \cdots & \rho'_{1n} \\ \rho'_{21} & 1 & \cdots & \rho'_{2n} \\ \vdots & \vdots & & \vdots \\ \rho'_{n1} & \rho'_{n2} & \cdots & 1 \end{bmatrix} \tag{A10}$$

According to the Nataf transformation, non-diagonal elements of $\boldsymbol{C}_{\boldsymbol{Y}}$ and $\boldsymbol{C}_\xi$ satisfy the following relations:

$$\rho'_{ij} = T\left(\rho_{ij}\right)\rho_{ij}\boldsymbol{C}_\xi = \begin{bmatrix} 1 & \rho'_{12} & \cdots & \rho'_{1n} \\ \rho'_{21} & 1 & \cdots & \rho'_{2n} \\ \vdots & \vdots & & \vdots \\ \rho'_{n1} & \rho'_{n2} & \cdots & 1 \end{bmatrix} \tag{A11}$$

It can be seen from the above analysis that once the standard normal distribution samples $\boldsymbol{\xi}$ and the correlation matrix $\boldsymbol{C}_\xi$ are obtained, the samples of $\boldsymbol{Y}$ with correlation matrix $\boldsymbol{C}_{\boldsymbol{Y}}$ can be obtained by using $Y_k = {F_k}^{-1}(\Phi(\xi_k))$.

Let $\boldsymbol{\eta} = [\eta_1, \eta_2, \dots, \eta_n]$ be the independent standard normal variables. A lower triangular matrix $\boldsymbol{B}$ is obtained by Cholesky decomposition of $\boldsymbol{C}_\xi$. Let

$$\xi = \begin{bmatrix} \xi_1 \\ \xi_2 \\ \vdots \\ \xi_n \end{bmatrix} = \boldsymbol{B}\boldsymbol{\eta} = \begin{bmatrix} b_{11} & & \\ \vdots & \ddots & \\ b_{n1} & \cdots & b_{nn} \end{bmatrix}\begin{bmatrix} \eta_1 \\ \eta_2 \\ \vdots \\ \eta_n \end{bmatrix} \tag{A12}$$

Thus, we can obtain the equation of random input variable $\boldsymbol{Y}$ expressed by independent random variables $\boldsymbol{\eta} = [\eta_1, \eta_2, \dots, \eta_n]$:

$$\boldsymbol{Y} = \boldsymbol{F}^{-1}(\boldsymbol{\Phi}(\boldsymbol{B}\boldsymbol{\eta})) \tag{A13}$$

References

[1] C. Wang, C. Lv, P. Li, et al. Modeling and optimal operation of community integrated energy systems: A case study from china. *Appl. Energy*, 230:1242–1254, 2018.

[2] L. Zhao, C. Wan, P. Yu, et al. Assessment of distributed photovoltaic hosting capacity in integrated electricity and heat systems considering uncertainty. *IET Energy Syst. Integr*, 3(3):317–326, 2021.

[3] Y. Xu, M. Korkali, L. Mili, et al. Risk assessment of rare events in probabilistic power flow via hybrid multi-surrogate method. *IEEE Trans. Smart Grid*, 11(2):1593–1603, 2019.

[4] J. Chen, T. Yu, Y. Xu, et al. Fast analytical method for reliability evaluation of electricity-gas integrated energy system considering dispatch strategies. *Appl. Energy*, 242:260–272, 2019.

[5] M. Zhu, C. Xu, S. Dong, et al. An integrated multi-energy flow calculation method for electricity-gas-thermal integrated energy systems. *Prot. Control Mod. Power Syst.*, 6(1):1–12, 2021.

[6] I. De Mel, O. V. Klymenko, and M. Short. Balancing accuracy and complexity in optimisation models of distributed energy systems and microgrids with optimal power flow: A review. *Sustainable Energy Technol. Assess.*, 52:102066, 2022.

[7] G. Von Wald, K. Sundar, E. Sherwin, et al. Optimal gas-electric energy system decarbonization planning. *Adv. Appl. Energy*, 6:100086, 2022.

[8] H. Yu, W. Tian, and J. Yan. Improved triangle splitting based bi-objective optimization for community integrated energy systems with correlated uncertainties. *Sustainable Energy Technol. Assess.*, 49:101682, 2022.

[9] X. Qin, X. Shen, Y. Guo, et al. Combined electric and heat system testbeds for power flow analysis and economic dispatch. *CSEE J. Power Energy Syst.*, 7(1):34–44, 2020.

[10] M. Yaghoubi-Nia, H. Hashemi-Dezaki, and A. H. Niasar. Optimal stochastic scenario-based allocation of smart grids' renewable and non-renewable distributed generation units and protective devices. *Sustainable Energy Technol. Assess.*, 44:101033, 2021.

[11] J. Zhao, J. Xiong, and H. Yu. Reliability evaluation of community integrated energy systems based on fault incidence matrix. *Sustainable Cities Soc.*, 80:103769, 2022.

[12] P. Li, S. Li, and H. Yu. Quantized event-driven simulation for integrated energy systems with hybrid continuous-discrete dynamics. *Appl. Energy*, 307:118268, 2022.

[13] A. M. L. da Silva and A. M. de Castro. Risk assessment in probabilistic load flow via monte carlo simulation and cross-entropy method. *IEEE Trans. Power Syst.*, 34(2):1193–1202, 2018.

[14] J. Bian, H. Wang, L. Wang, et al. Probabilistic optimal power flow of an ac/dc system with a multiport current flow controller. *CSEE J. Power Energy Syst.*, 7(4):744–752, 2020.

[15] S. Bao, Z. Yang, J. Yu, et al. Probabilistic energy flow and risk assessment of electricity–gas systems considering the thermodynamic process. *Energy*, 189:116263, 2019.

[16] S. Chen, Z. Wei, G. Sun, et al. Multi-linear probabilistic energy flow analysis of integrated electrical and natural-gas systems. *IEEE Trans. Power Syst.*, 32(3):1970–1979, 2016.

[17] N. Luthen, S. Marelli, and B. Sudret. Sparse polynomial chaos expansions: Literature survey and benchmark. *SIAM-ASA J. Uncertain. Quantif.*, 9(2):593–649, 2021.

[18] Q. Hu, B. Zeng, Y. Zhang, et al. Analysis of probabilistic energy flow for integrated electricity-gas energy system with p2g based on cumulant method. In *Proc. IEEE Conf. Energy Internet Energy Syst. Integr. (EI2)*, pages 1–6. IEEE, 2017.

[19] Y. Li, W. Li, W. Yan, et al. Probabilistic optimal power flow considering correlations of wind speeds following different distributions. *IEEE Trans. Power Syst.*, 29(4):1847–1854, 2014.

[20] S. Rajamand. Feedback-based control structure for frequency/voltage regulation using the state of electrical vehicle charge station and point estimation method. *Sustainable Energy Technol. Assess.*, 51:101922, 2022.

[21] H. R. Massrur, T. Niknam, and M. Fotuhi-Firuzabad. Investigation of carrier demand response uncertainty on energy flow of renewable-based integrated electricity–gas–heat systems. *IEEE Trans. Ind. Informat.*, 14(11):5133–5142, 2018.

[22] D. Huang, H. Li, G. Cai, et al. An efficient probabilistic approach based on area grey incidence decision making for optimal distributed generation planning. *IEEE Access*, 7:93175–93186, 2019.

[23] Y. Hu, H. Lian, Z. Bie, et al. Unified probabilistic gas and power flow. *J. Modern Power Syst. Clean Energy*, 5(3):400–411, 2017.

[24] D. Xiu and G. E. Karniadakis. Modeling uncertainty in steady state diffusion problems via generalized polynomial chaos. *Comput. Meth. Appl. Mech. Eng.*, 191(43):4927–4948, 2002.

[25] H. Wu, Y. Zhou, S. Dong, et al. Probabilistic load flow based on generalized polynomial chaos. *IEEE Trans. Power Syst.*, 32(1):820–821, 2016.

[26] H. Wu, D. Shen, B. Xia, et al. Parametric problems in power system analysis: recent applications of polynomial approximation based on galerkin method. *J. Mod. Power Syst. Clean Energy*, 9(1):1–12, 2020.

[27] Y. Xu, L. Mili, A. Sandu, et al. Propagating uncertainty in power system dynamic simulations using polynomial chaos. *IEEE Trans. Power Syst.*, 34(1):338–348, 2018.

[28] G. Wang, H. Xin, D. Wu, et al. Data-driven arbitrary polynomial chaos-based probabilistic load flow considering correlated uncertainties. *IEEE Trans. Power Syst.*, 34(4):3274–3276, 2019.

[29] X. Zhang, M. D. Pandey, and H. Luo. Structural uncertainty analysis with the multiplicative dimensional reduction–based polynomial chaos expansion approach. *Struct. Multidiscip. Optim.*, 64(4):2409–2427, 2021.

[30] G. Blatman and B. Sudret. Adaptive sparse polynomial chaos expansion based on least angle regression. *J. Comput. Phys.*, 230(6):2345–2367, 2011.

[31] X. Liu. *Combined analysis of electricity and heat networks*. PhD thesis, Cardiff Univ., 2013.

[32] A. Shabanpour-Haghighi and A. R. Seifi. An integrated steady-state operation assessment of electrical, natural gas, and district heating networks. *IEEE Trans. Power Syst.*, 31(5):3636–3647, 2015.

[33] A. Martinez-Mares and C. R. Fuerte-Esquivel. A unified gas and power flow analysis in natural gas and electricity coupled networks. *IEEE Trans. Power Syst.*, 27(4):2156–2166, 2012.

[34] C. M. Correa-Posada and P. Sanchez-Martin. Integrated power and natural gas model for energy adequacy in short-term operation. *IEEE Trans. Power Syst.*, 30(6):3347–3355, 2014.

[35] P. Li, B. Dong, H. Yu, et al. A unified energy bus based multi-energy flow modeling method of integrated energy system. *Energy Procedia*, 159:418–423, 2019.

[36] S. Peng, J. Tang, and W. Li. Probabilistic power flow for ac/vsc-mtdc hybrid grids considering rank correlation among diverse uncertainty sources. *IEEE Trans. Power Syst.*, 32(5):4035–4044, 2016.

[37] D. Xiu. *Numerical methods for stochastic computations: a spectral method approach*. PhD thesis, Princeton Univ., 2010.

[38] Y. Xu, L. Mili, and J. Zhao. Probabilistic power flow calculation and variance analysis based on hierarchical adaptive polynomial chaos-anova method. *IEEE Trans. Power Syst.*, 34(5):3316–3325, 2019.

[39] P. Tsilifis, X. Huan, C. Safta, et al. Compressive sensing adaptation for polynomial chaos expansions. *J. Comput. Phys.*, 380:29–47, 2019.

[40] B. Zhang and Y. Ni. A hybrid sequential sampling strategy for sparse polynomial chaos expansion based on compressive sampling and bayesian experimental design. *Comput. Methods Appl. Mech. Eng.*, 386:114130, 2021.

[41] S. D. Babacan, R. Molina, and A. K. Katsaggelos. Bayesian compressive sensing using laplace priors. *IEEE Trans. Image Process.*, 19(1):53–63, 2009.

[42] L. Ye, J. Yao, X. Ouyang, et al. Risk analysis and utility function-based decision-making model for spinning reserve allocations. *IEEE Access*, 9:18752–18761, 2021.

[43] R. A. Jabr. Distributionally robust cvar constraints for power flow optimization. *IEEE Trans. Power Syst.*, 35(5):3764–3773, 2020.

[44] X. Chen, W. Wu, and B. Zhang. Robust restoration method for active distribution networks. *IEEE Trans. Power Syst.*, 31(5):4005–4015, 2015.

[45] S. Wu, R. Z. Rios-Mercado, E. A. Boyd, et al. Model relaxations for the fuel cost minimization of steady-state gas pipeline networks. *Math. Comput. Model*, 31(2-3):197–220, 2000.

[46] O. Ciftci, M. Mehrtash, and A. Kargarian. Data-driven nonparametric chance-constrained optimization for microgrid energy management. *IEEE Trans. Ind. Inf.*, 16(4):2447–2457, 2019.

[47] S. Rahman, M. A. Khallat, and Z. M. Salameh. Characterization of insolation data for use in photovoltaic system analysis models. *Energy*, 13(1):63–72, 1988.

[48] J. A. Carta, P. Ramirez, and S. Velazquez. A review of wind speed probability distributions used in wind energy analysis: Case studies in the canary islands. *Renewable and sustainable energy rev.*, 13(5):933–955, 2009.